*metals*

MDPI

*Article*

# Ceramic Conversion Treatment of Commercial Pure Titanium with a Pre-Deposited Vanadium Layer

**Zhenxue Zhang *, Rui Deng and Hanshan Dong**

School of Metallurgy and Materials, University of Birmingham, Birmingham B15 2TT, UK; rxd089@alumni.bham.ac.uk (R.D.); h.dong.20@bham.ac.uk (H.D.)
* Correspondence: z.zhang.1@bham.ac.uk

**Abstract:** Titanium is characterized by poor wear resistance which restricts its application. Ceramic conversion treatment (CCT) is used to modify the surface; however, it is a time-consuming process. In this work, a thin vanadium layer was pre-deposited on the commercial pure titanium (CPTi) samples' surface, and it increased the oxygen absorption significantly and assisted in obtaining a much thicker oxide layer than those samples without a V layer at the treatment temperatures of 620 °C and 660 °C. The oxidation of the samples pre-deposited with the V layer had a much higher oxidation rate, and V was evenly distributed in the oxide layer. After CCT, all samples had a low wear volume and stable coefficient of friction in comparison to the untreated CPTi sample. A slightly higher wear area in the wear track was observed on the V pre-deposited samples than those samples without vanadium, especially those with a thicker oxide layer (>4 μm). This might be associated with defects in a thicker oxide layer and insufficient support from a shallower oxygen diffusion zone or hard debris created at the initial stage. Vanadium in the oxide layer reduced the contact angles of the surface and increased the wettability significantly.

**Keywords:** titanium; vanadium; oxidation; ceramic conversion treatment



**Citation:** Zhang, Z.; Deng, R.; Dong, H. Ceramic Conversion Treatment of Commercial Pure Titanium with a Pre-Deposited Vanadium Layer. *Metals* **2023**, *13*, 1859. https://doi.org/10.3390/met13111859

Academic Editor: Antonio Mateo

Received: 2 October 2023
Revised: 1 November 2023
Accepted: 3 November 2023
Published: 7 November 2023



## 1. Introduction

Thanks to their excellent combination of low density, high strength-to-weight ratio, superior corrosion resistance, and bio-compatibility, titanium alloys are employed in components like bioimplants [1], auto engine parts, fan blades in aero-engines, and so on [2]. However, severe adhesive wear and unstable friction limit their applications under load [3]. In order to improve their mechanical performance, modifications to the surface of titanium alloys are essential via various methods, like physical vapor deposition (PVD), chemical vapor deposition (CVD), thermal spraying, ion implantation, thermal oxidation, and laser surface modification [4,5]. However, certain issues need to be addressed when applying these techniques. For instance, in terms of coating techniques, inherent oxide film on the surface causes weak bonding between coating and substrate, leading to low load-bearing capacity [6]. Ceramic conversion treatment (CCT) is an environmentally friendly and low-cost technique that aims to improve the tribological properties of titanium alloys by forming a thin and compact oxide layer supported by a diffusion zone [1,7]. Recently, fast CCT was developed to shorten the treatment time and save energy by pre-depositing a metal layer like gold or silver to accelerate the process [8,9]. Vanadium (V) is a β stabilizer in titanium alloys. In contrast to aluminum, although vanadium is expensive and toxic to the human body [10,11], it generally speeds up the oxidation of titanium to produce a larger surface area which is beneficial for the photocatalytic property, etc. [12]. As an alloying element in Ti6Al4V alloy, vanadium plays an important role in the accelerated oxidation of Ti6Al4V with Ag [9]. However, whether a pre-deposited vanadium layer can enhance the ceramic conversion process of titanium alloys is questionable, which forms the topic of this research.

The lubrication of the materials is strongly linked to the wettability of the surface, which can be quantified by the contact angle between the surface and liquid drops [3]. On top of that, the switch between extremely hydrophilic or hydrophobic surfaces, triggered by certain specific stimulation, is critical in many applications, like self-cleaning, anti-corrosion, and liquid transportation applications [13].

In this work, based on previous experience, we investigated the impact of a pre-deposited V layer on the CCT of CPTi at 620/660 °C for 8 or 80 h. In the meantime, the microstructure, mechanical, wettability, and tribological performance of the modified layer were investigated to develop an efficient technique for a functional surface.

## 2. Materials and Methods

A commercial pure titanium (CPTi) grade 2 rod with a diameter of 25.4 mm was cut using a silicon carbide blade into 4.5 mm thick small cylinder-shaped coupons. The coupons were gradually ground from 120, 240, 400, 800 to 1200 grit sequentially, then they were immersed in an acetone bath to apply ultrasonic cleaning, followed by drying under hot air. After CCT, samples were sectioned and mounted in conductive Bakelite in an OPAL 460 machine (MetPrep Ltd., Coventry, UK) and ground progressively to 2400 grit before polishing using activated colloidal silica to a mirror-like finish. Kroll's reagent, comprising 2%HF + 10%$HNO_3$ + balanced water, was employed to reveal the microstructures.

The pre-depositing of V layers was conducted on a Close Field Unbalanced Magnetron Sputtering Ion Plating equipment (Teer Coating Ltd., Drotwich, UK) at 1.5 A for 5 min to obtain a layer about 50–100 nm thick. Ceramic conversion treatments (CCT) were conducted in an Elite Thermal Systems Limited electric furnace with a ramp rate of 8 °C/min and a furnace cooling rate of 2 °C/min. Three conditions at 620 °C for 8 h, 660 °C for 8 h, and 620 °C for 80 h were carried out to compare the temperature and duration effect. The corresponding sample code represents the relative CCT condition. For example, C-V620/8 stands for a CPTi sample pre-deposited with V and CCT at 620 °C for 8 h, while a C-620/8, a sample without a V layer, underwent the same CCT. Samples before and after coating and CCT were weighed by an OHAUS GALAXY 160D balance (Ohaus corporation, Parsippany, NJ, USA) to estimate the metallic layer thickness and oxygen absorption. The mass change was also monitored continuously for 15 h in a NETZSCH STA 449C thermogravimetric (Netzsch thermal Instruments UK, Ltd., Wolverhampton, UK) to compare the mass gain process of the sample with or without the vanadium layer. The test includes heating a 5 mm × 5 mm × 1 mm disc sample with a ramp period of 75 min at 8 °C/min from room temperature to 620 °C and held for 15 h. An XP-200 Plus TYLUS 3D profilometer (Tylus Enterprise Pte Ltd, Singapore, Singapore) was used to assess the roughness of arithmetical mean height (Ra) with 10 measurements at different locations.

A PROTO AXRD benchtop powder diffraction system equipment (XRD, Proto, Crewe, UK) was employed for identifying surface phases and constituents. The diffraction data were analyzed using an X-Pert Highscore program with the PCPDFWIN database (Panalytical B.V., Almelo, the Netherlands). The morphology and microstructure of the surface and cross-section were observed via a Jeol 7000 scanning electron microscope (SEM, JEOL Ltd., Tokyo, Japan) equipped with an Oxford Aztec energy dispersive X-ray spectroscopy (SEM/EDX, Jeol, Welwyn Garden City, UK) to collect elemental information.

The samples' surface microhardness was tested on a Zwick/Roell microhardness machine (ZwickRoell Ltd., Worcester, UK) with a load of 25 gf and a holding time of 10 s using Vickers indenter. The cross-section hardness profiles in the depth of the samples were measured on the same equipment via the Knoop indenter under a load of 25 gf. Tribological properties were tested in a Phoenix TE-79 multi-axis tribology machine (Phoenix Tribology Ltd, Kingsclere, UK). The reciprocating friction and wear test was carried out for 1000 cycles over 5 mm, with a sliding speed of 5 mm/s under a load of 40 N against a WC ball, which has a diameter of 8 mm. Wear track profiles were plotted by an XP-200 Plus TYLUS 3D-profilometer to calculate the wear areas. In addition, SEM and EDX were also used to obtain the morphology and elemental information of the tracks.

MicroCapture Plus software (V3.1, ProScope Digital, Wilsonville, OR, USA) was used to capture pictures of water drops for wettability tests. Each drop contained 5 µL of water, and drops were evenly distributed in 5 different positions on the samples' surface. Contact angles were analyzed by Ossila Contact Angle software (version 1.3.0, Ossila, Sheffield, UK).

## 3. Results

### *3.1. Surface Morphology Change*

A metallic luster can be seen on the surface of the as-ground CPTi sample (Figure 1a). After CCT at 620 °C for 8 h, the surface of CPTi became brownish (Figure 1b), and it turned to grey after 80 h treatment (Figure 1c), while it transformed darker after CCT at 660 °C/8h (Figure 1d). The CPTi samples appeared slightly metallic grey colored after pre-deposited with a very thin vanadium layer (Figure 1e). After 8 h of CCT at 620 °C, sample C-V620/8 grew much darker than that of C-620/8, however, it appeared less dark after 80 h of treatment (Figure 1g), though it was darker than that of C-620/80. A similar color emerged on sample C-V660/8 in Figure 1h.

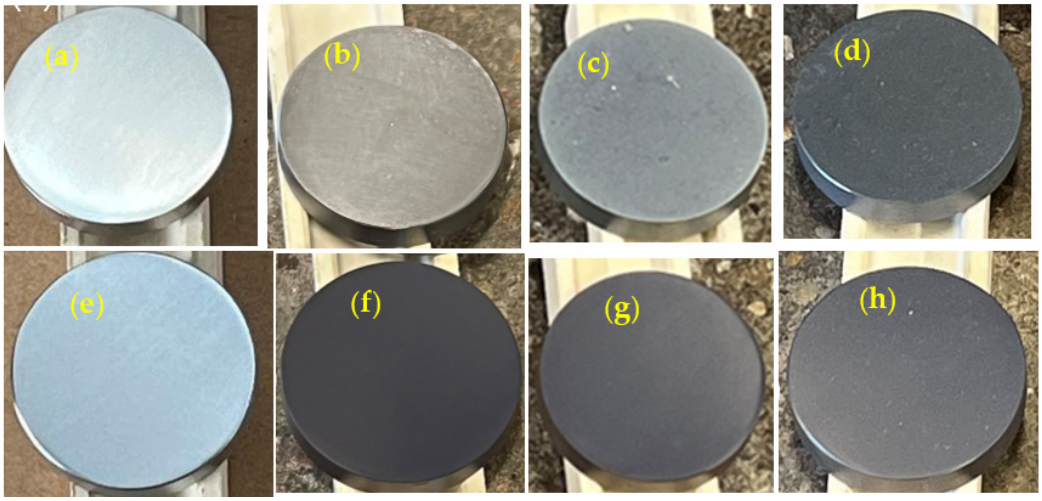


**Figure 1.** Images of sample coupons (Ø25.4 mm) before and after CCT: (**a**) CPTi; (**b**) C-620/8; (**c**) C-620/80; (**d**) C-660/8; (**e**) CPTi pre-deposited with a V layer; (**f**) C-V620/8; (**g**) C-V620/80; and (**h**) C-V660/8.

Grinding marks were still clear and visible on all types of samples after CCT, as demonstrated in Figure 2. After CCT for 8 h at 620 °C and 660 °C, the grinding marks on the C-620/8 and C-660/8 samples did not change much. However, extending the treatment time to 80 h (C-620/80), the surface turned out smoother with shallow marks and blurred edges (Figure 2b). For the V pre-deposited samples, similar surface morphology development was observed, as demonstrated in Figure 2d–f. Without the vanadium pre-deposited layer, the surface became slightly rougher with the increment of temperature and duration, as shown in Figure 3. The Ra value became much higher after CCT for samples with a pre-deposited V layer. For example, sample C-V660/8 doubled its Ra value to 0.45 µm in comparison to 0.22 µm for C-660/8 h.

### *3.2. Oxidation Kinetics and Mass Gain after CCT*

The oxidation kinetics of the CPTi and vanadium pre-deposited samples were examined by a thermogravimetric test to monitor the mass change for 15 h, as shown in Figure 4. Although the titanium sample with a pre-deposited vanadium layer increased slower in the 75 min ramp period than the CPTi sample, the mass gain was clearly higher at the holding period with a total gain of 0.38% (C-V620/15) in comparison to a 0.15% increment for C-620/15.

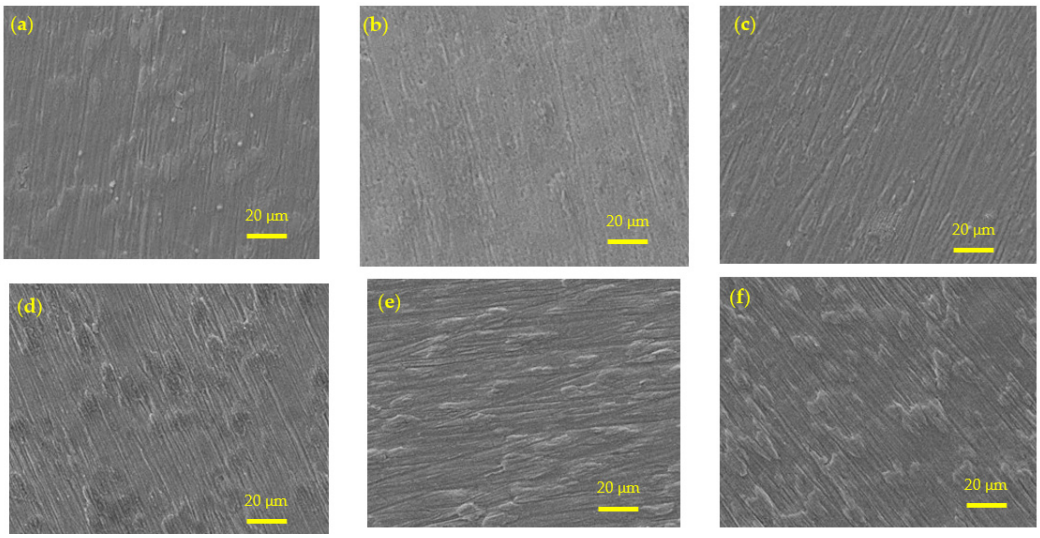


**Figure 2.** Surface morphology of samples after CCT: (**a**) C-620/8, (**b**) C-620/80, (**c**) C-660/8, (**d**) C-V620/8, (**e**) C-V620/80, and (**f**) C-V660/8.

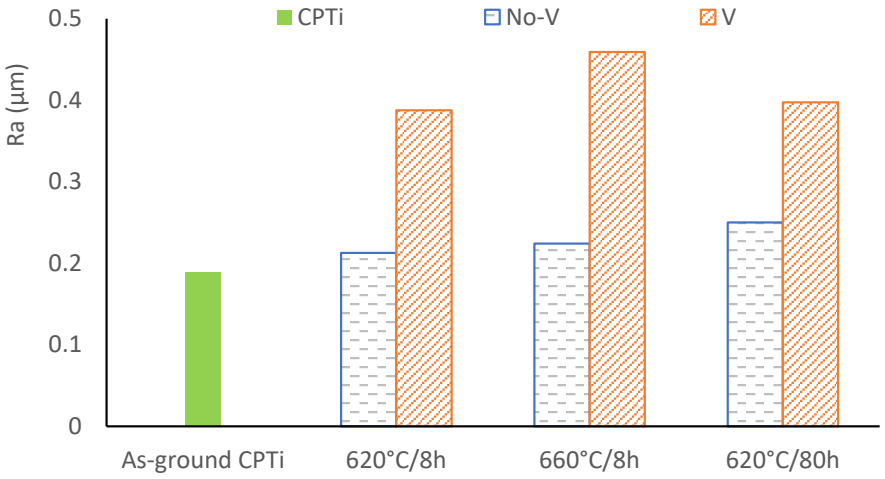


**Figure 3.** Surface roughness (Ra) changes of the samples after CCT.

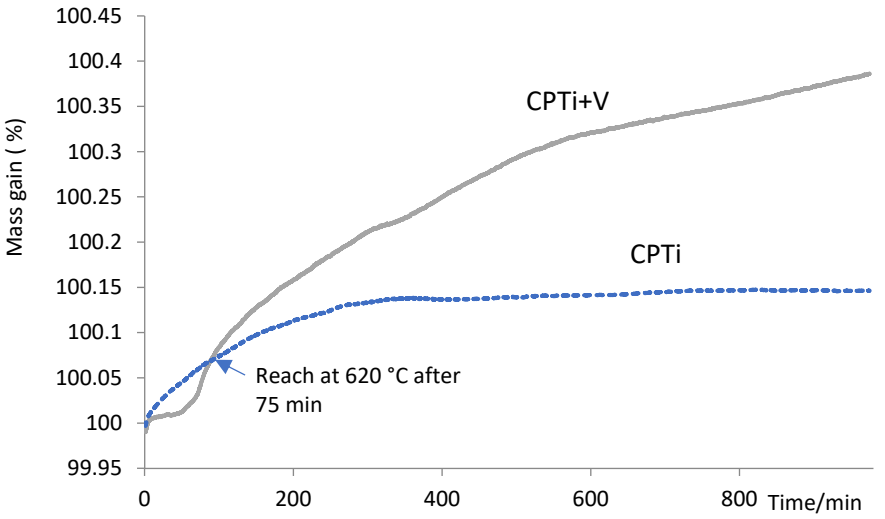


**Figure 4.** Mass gain of the CPTi samples (5 mm × 5 mm × 1 mm thick disc) with or without the pre-deposited vanadium layer as a function of the oxidation time in a thermogravimetric test (TGA).

After PVD, a very thin layer was attached to the samples, as indicated in Table 1. The thickness was calculated by the mass gain after deposition, divided by the surface area covered, times the density of vanadium, and the average value was 0.1 μm. Samples with pre-deposited V layers absorbed more oxygen compared to those samples treated at the same condition, indicating accelerated oxidation from V addition, as seen in Table 1. After CCT, the mass gain of sample C-V620/8 (6.5 mg) was twice that of sample C-620/8. After increasing the temperature of CCT from 620 to 660 °C, for the same duration of 8h, there was about 5.7 mg for C-660/8 and 8.7 mg for C-V660/8. In terms of the long duration of 80 h, the oxygen absorption of samples with a pre-deposited V layer (C-V620/80) demonstrated a much higher absorption (14.4 mg) than C-620/80 (9.6 mg).

**Table 1.** Sample detail and mass change through the treatment.

| | Calculated V Layer Thickness (μm) | Before CCT (g) | After CCT (g) | Mass Gain (mg) |
|---|---|---|---|---|
| C-620/8 | - | 10.5438 | 10.5469 | 3.1 |
| C-V620/8 | 0.065 | 10.2450 | 10.2515 | 6.5 |
| C-620/80 | - | 10.3976 | 10.4072 | 9.6 |
| C-V620/80 | 0.101 | 10.3504 | 10.3648 | 14.4 |
| C-660/8 | - | 10.2636 | 10.2693 | 5.7 |
| C-V660/8 | 0.097 | 10.5205 | 10.5294 | 8.9 |

The cross-sectional microstructure of the oxide layer was observed under SEM and the thickness of the oxide layer was also measured at 5–10 points to obtain an average value. As shown in Figure 5a, a very thin and dense oxide layer (about 0.8 μm) covered the surface of C-620/8 with a roughly 7–10 μm oxygen diffusion zone up to the dashed line in Figure 5a. A thicker and relatively dense oxide, about 3.6 μm, was formed on the surface of sample C-V620/8 (Figure 5d). However, the oxygen diffusion zone was about the same for samples C-620/8 and C-V620/8. Extending the treatment to 80 h, the oxide layer on C-620/80 was about 2.7 μm thick and still quite dense (Figure 5b), which was less thick than that of C-V620/8. Meanwhile, the oxide layer of C-V620/80 grew to 7.1 μm, composed of a loose top layer and dense under layer. The oxygen diffusion zone for samples C-620/80 and C-V620/80 was deeper (20–25 μm) beneath the oxide layer. Raising the temperature to 660 °C, the oxide layer (1.6 μm) of C-660/8 doubled to that of C-620/8 and remained dense, while the diffusion zone for C-660/8 was also expanded. In the meantime, the thickness of the oxide layer on sample C-V660/8 was 3.8 μm, which was more than twice that of C-660/8 (Figure 5c,f), but it was much less dense. Without vanadium, the oxide layers were generally compact and dense (Figure 5a–c). With a pre-deposited V layer, the oxide was compact and dense on C-V620/8. However, it became loose and porous on the surface when the oxide layer became much thicker for C-V620/80 and C-V660/8.

A detailed EDX analysis of the cross-section of the sample is demonstrated in Figure 6. The dark zone in the top loose oxide layer (Spectrum 1) had more vanadium and less oxygen than the bright zone (Spectrum 2) in the Backscattering electron image. The underlayer was dense with a similar O/Ti ratio near the stoichiometric of $TiO_2$ (Spectrum 3 and 6). The oxygen content gradually reduced from spectrum 4 to spectrum 5 with the increment of depth.

The thickness of these oxide layers was plotted together with previous test data (as shown in Figure 7). The oxide layer increased significantly higher for the CPTi samples with a pre-deposited vanadium layer than those without a vanadium layer at 620 °C and 660 °C.

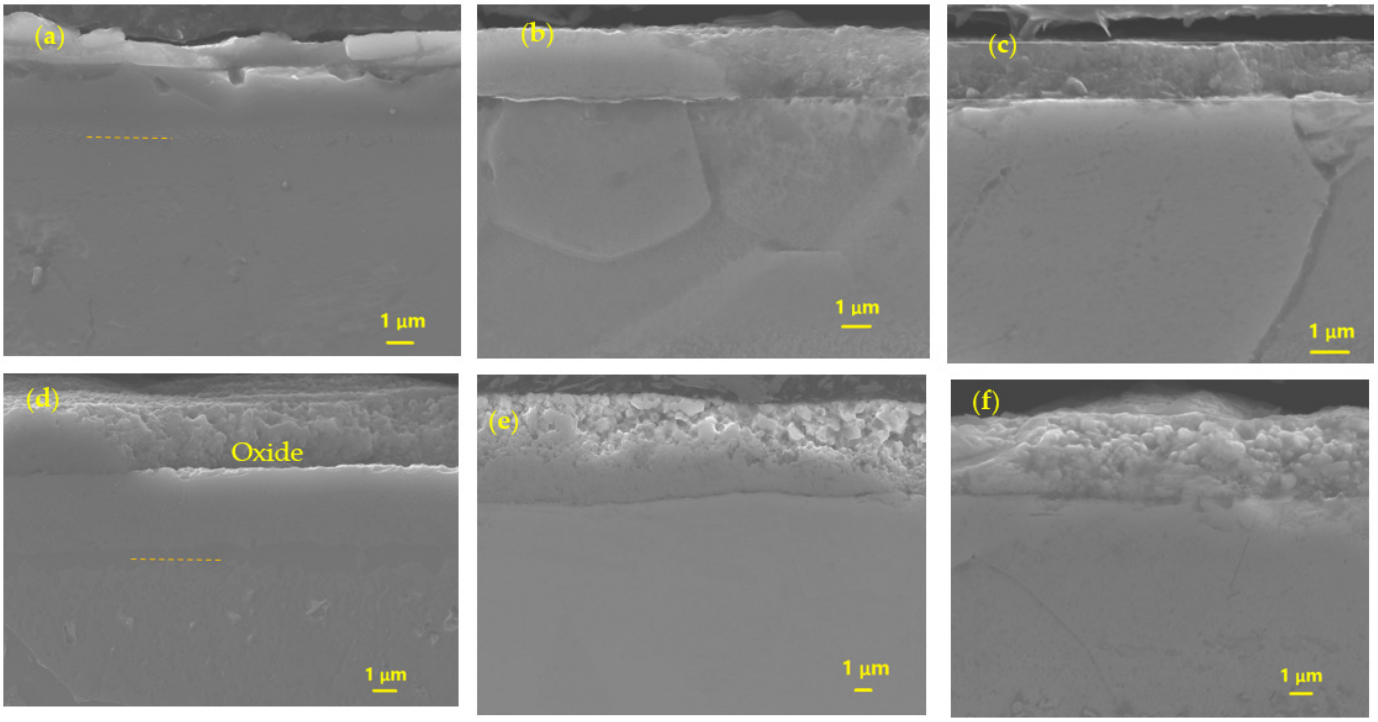


**Figure 5.** Cross-sectional SEM images of samples: (**a**) C-620/8; (**b**) C-620/80, (**c**) C-660/8, (**d**) C-V620/8, (**e**) C-V620/80, and (**f**) C-V660/8.

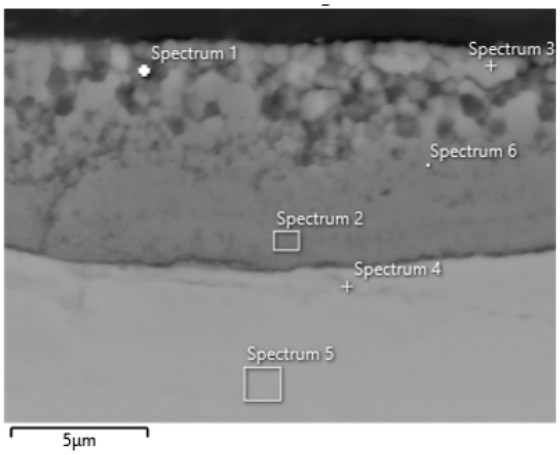


| Atomic % | 1 | 2 | 3 | 4 | 5 | 6 |
|---|---|---|---|---|---|---|
| O | 57.26 | 65.49 | 67.6 | 36.76 | 23.01 | 63.46 |
| Al | 0 | 0.18 | 0.2 | 0.19 | 0.25 | 0.17 |
| Ti | 41.17 | 34.12 | 30.96 | 63.05 | 76.73 | 35.57 |
| V | 1.57 | 0.21 | 1.24 | 0 | 0 | 0.81 |

**Figure 6.** EDX analysis of the cross-sectional SEM images of sample C-V620/80.

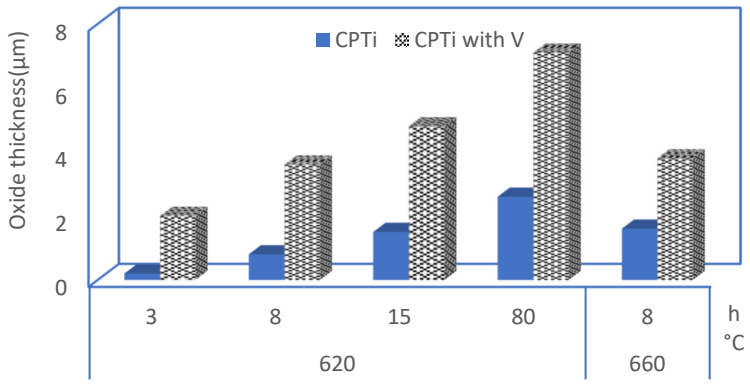


**Figure 7.** Change of the thickness of the oxide layer with CCT time, including previous test results.

### *3.3. Surface Phase Constituent Change*

The surface phase constituent's evolution after different CCTs is revealed in Figure 8. The rutile oxide peaks grew on the CPTi surface with elevated temperature and extended duration, while the peaks of the α-phase weakened and shifted slightly to the lower angle direction due to the dissolution of oxygen. A stronger intensity of $TiO_2$ indicated that samples with the pre-deposited V layer generated more rutile $TiO_2$. There was almost no anatase detected for all the samples. For C-V620/8, C-V660/8, and C-V620/80, there was no vanadium oxide peak identified.

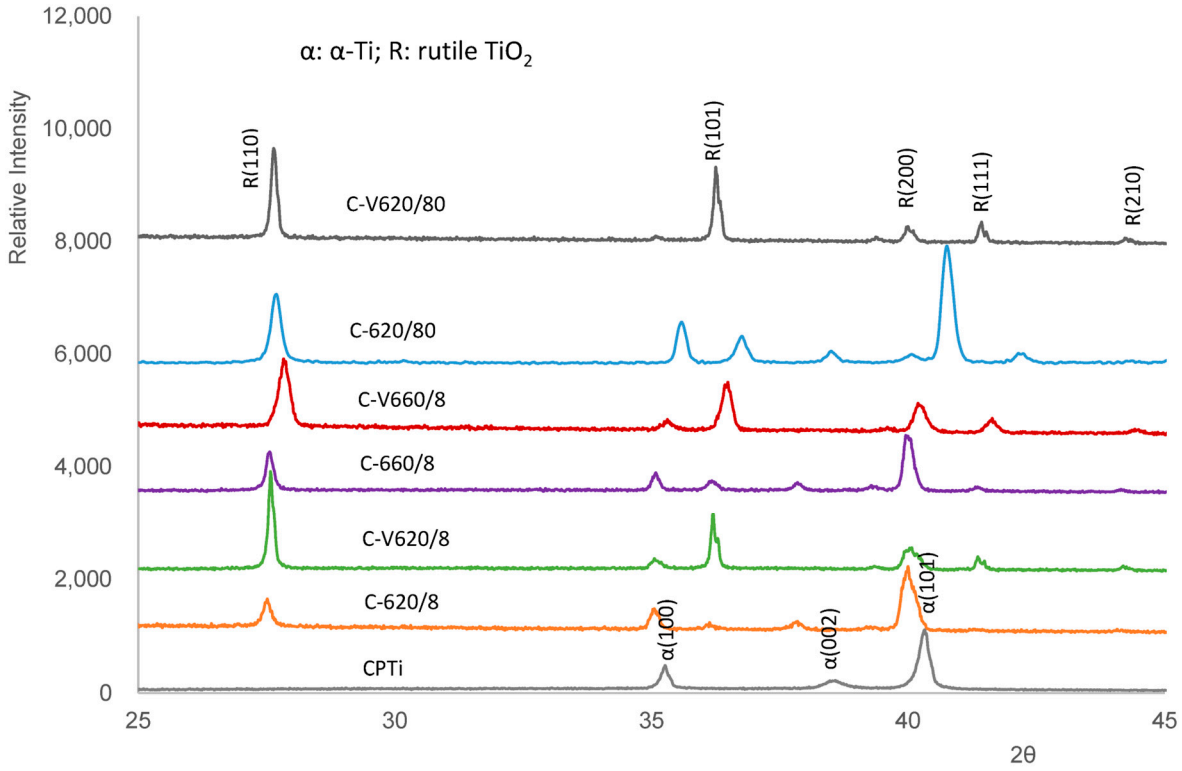


**Figure 8.** Phase constituent evolution of the CPTi sample after different treatments.

### *3.4. Surface and Cross-Sectional Hardness*

After CCT, the surface hardness increased markedly than that of the untreated sample ($HV_{0.025}$ 220), as recorded in Figure 9. For the duration of 8 h, with temperature rising to 660 °C from 620 °C, the hardness value increased slightly from $HV_{0.025}$ 560 for C-620/8 to $HV_{0.025}$ 624 for C-660/8. Meanwhile, the surface with vanadium was only marginally harder than that of the surface without vanadium. In terms of the long duration of 80 h, a notable enhancement in hardness was observed for both C-620/80 ($HV_{0.025}$ 800) and C-V620/80 ($HV_{0.025}$ 841).

The Knoop indenter was used to measure the microhardness of the diffusion zone under the oxide layer, as indicated in Figure 10. The hardness value drops rapidly near the surface region for the treatment of 8 h with a depth under 10 μm, indicating a shallow oxygen-enriched zone. The hardness value for sample C-V660/8 was slightly higher and deeper. For a longer treatment, the harder zone was between 20 and 30 μm, suggesting a deeper oxygen diffusion length in the substrate as hardness is proportional to the oxygen content in the titanium.

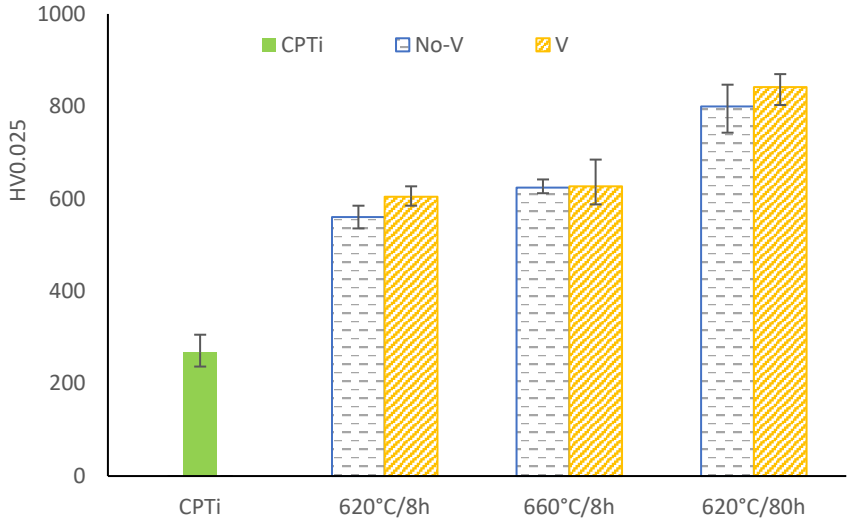


**Figure 9.** Surface hardness using a Vickers indenter under a load of 25 gf.

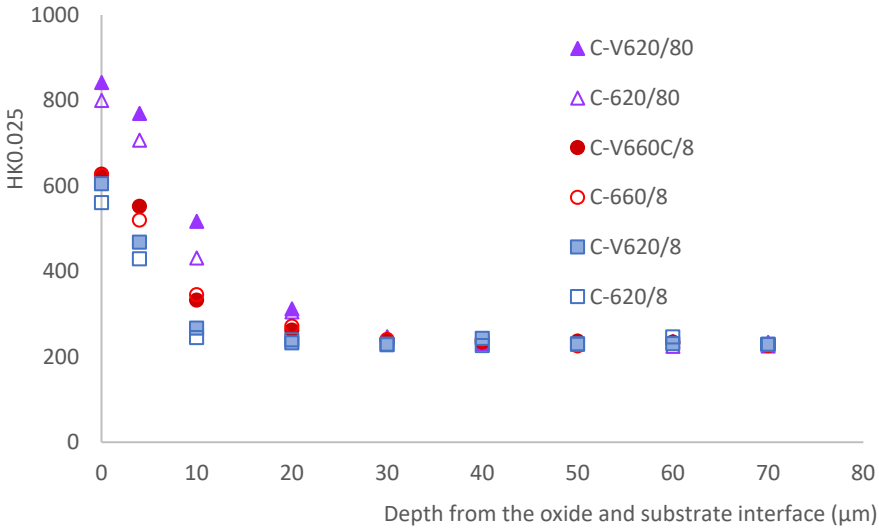


**Figure 10.** Cross-sectional hardness under the oxide layer measured by a Knoop indenter under a load of 25 gf.

### *3.5. Friction and Wear*

As demonstrated in Figure 11, CPTi had a very high coefficient of friction (CoF) in the first contact with the WC ball, and it dropped gradually in the first 200 cycles and then climbed again till the end. There was also a large range of fluctuation of CoF in the whole 3000 test cycles, indicating an unstable contact. All samples with oxide layers had a lower initial CoF at about 0.1, but they increased significantly in a short period. In terms of samples without a pre-deposited layer, the CoF of C-620/8 and C-620/80 rose relatively fast in the first 200 cycles before reaching a mild increase range. However, the CoF of C-660/8 grew rather mildly in the first 270 cycles and then surged to a level like that of C-620/8 and C-620/80. For the V pre-deposited samples, a sharp growth of CoF at the beginning was found, especially for samples C-V620/8 and C-V620/80 (Figure 11), and then the CoF for C-V620/80 and C-V660/8 increased steadily till the end. However, the CoF for sample C-V620/8 maintained almost unchanged at around 0.28 from about 30 to 1000 cycles.

After the tribo-test, the wear track was plotted by a profilometer, and the wear area was measured. As shown in Figure 12a, after the tribological test, a wide and deep wear track was created on the surface of the CPTi sample, while a much smaller track was formed on the surface of C-V660/8 and the C-660/8 had the smallest wear area. For CCT at other

temperatures and times, the CCTed samples with the V pre-deposited layer also had a larger and deeper wear track, as evidenced in the wear area comparison in Figure 12b.

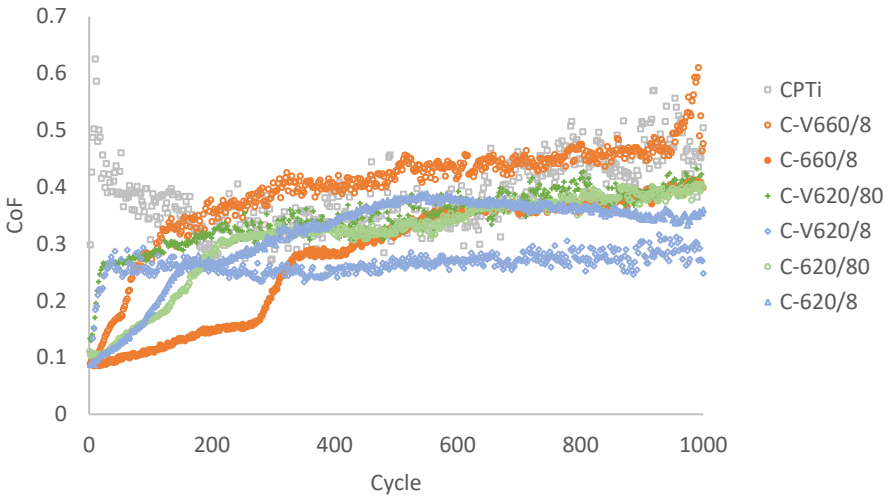


**Figure 11.** CoF change of sample under a load of 40 N.

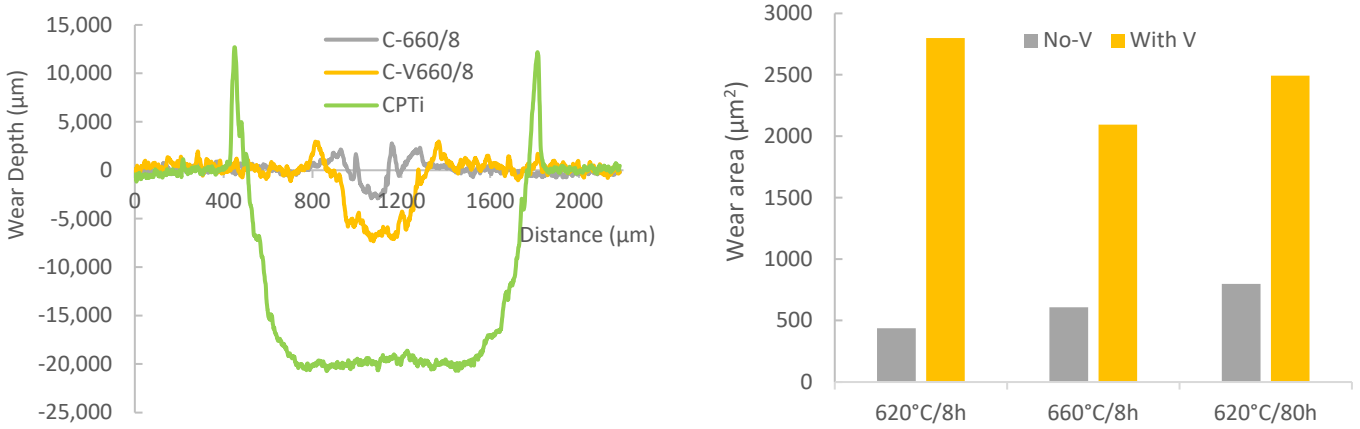


(**a**) (**b**)

**Figure 12.** (**a**) Typical wear tracks on untreated and CCTed samples (660 °C/8 h) and (**b**) comparison of the average wear area of the wear tracks.

The wear tracks were examined by SEM/EDX, as shown in Figure 13 and Table 2. As evidenced in the EDX results, part of the oxide layer in the track of both samples C-660/8 and C-V660/8 was removed after the tribo-test. Scratched grooves were still observed for sample C-V660/8 with the pre-deposited V layer. Spallation occurred on the surface of other CCTed samples, as shown in Figure 14, suggesting the oxide layer could be worn through at current test conditions.

**Table 2.** EDX analysis on the composition of the track and the surface.

| Sample | at % | Ti | O | V | W | C |
|---|---|---|---|---|---|---|
| C-660/8 | 1 | 61.11 | 36.79 | - | 0.03 | 2.07 |
| | 2 | 33.39 | 66.61 | - | | |
| C-V660/8 | 1 | 71.37 | 25.63 | 0.08 | 0.02 | 2.90 |
| | 2 | 66.53 | 30.03 | 0.29 | 0.05 | 3.10 |
| | 3 | 31.27 | 66.96 | 1.77 | | |

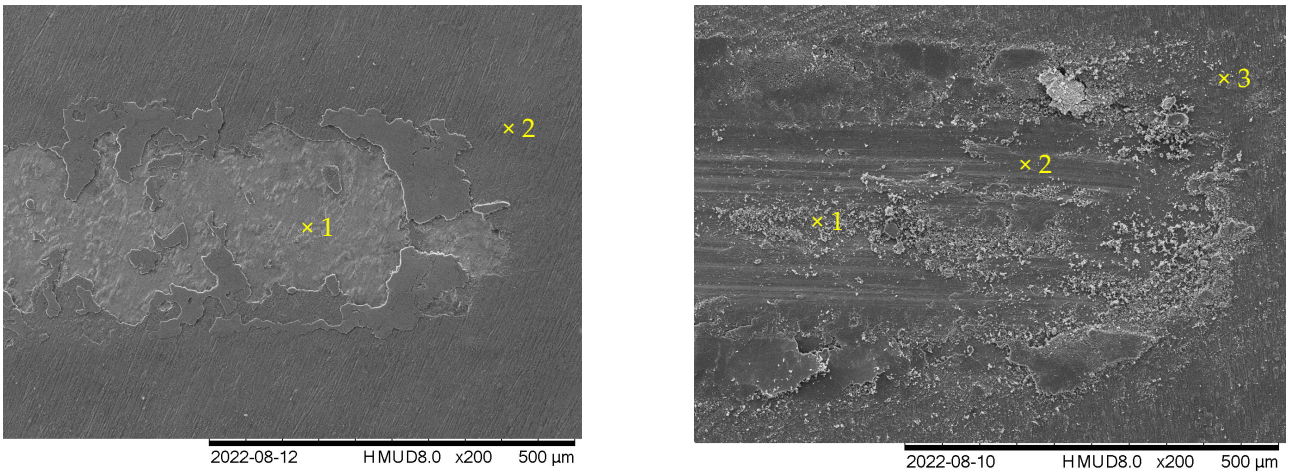


(**a**) (**b**)

**Figure 13.** SEM images of wear tracks: (**a**) C-660/8; (**b**) C-V660/8.

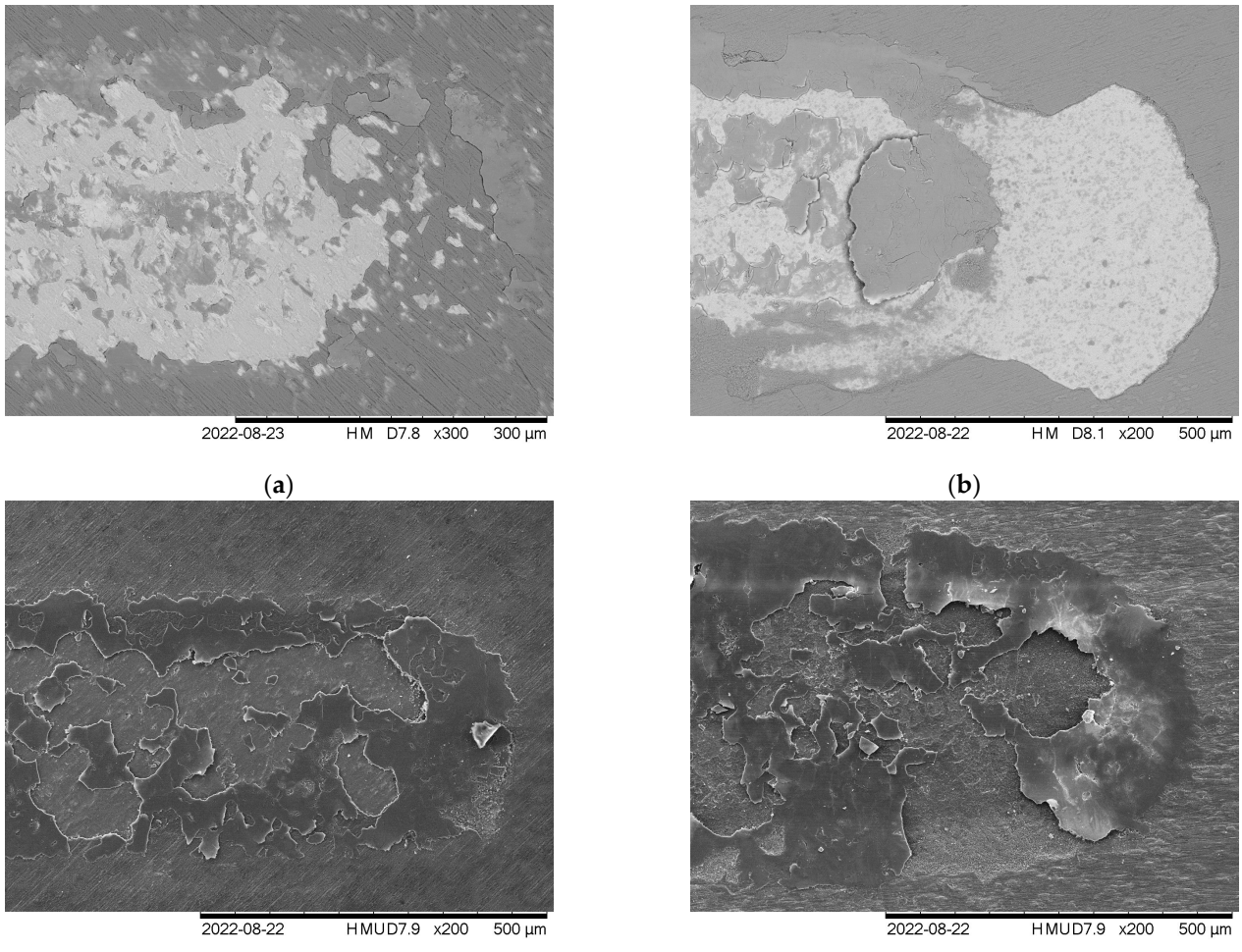


(**a**) (**b**)

(**c**) (**d**)

**Figure 14.** SEM images of wear tracks: (**a**) C-620/8, (**b**) C-V620/8, (**c**) C-620/80, and (**d**) C-V620/80.

### *3.6. Wettability*

Vanadium had a significant impact on the wettability of the surface of CPTi. After CCT, the contact angle increased, especially for C-620/8, which was over 80° in comparison to about 55° for an untreated surface (Figure 15). However, for the V pre-deposited sample,

the contact angle θ went down after CCT, and it decreased further with the growth of temperature and duration (Figure 15). It suggested that rapid CCT, prompted by V, led to good surface wettability.

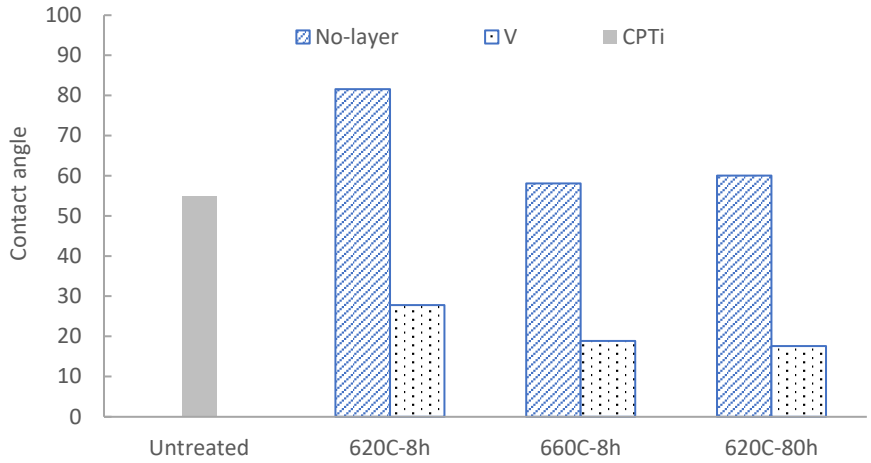


**Figure 15.** Contact angle of samples after different treatments.

## 4. Discussion

### *4.1. Oxidation Mechanism of Titanium with Vanadium*

The impact of vanadium on the oxidation behavior of titanium was investigated at three CCT conditions of 620 °C for 8 h, 660 °C for 8 h, or 620 °C for 80 h. Active oxygen molecules collide with the titanium surface and are absorbed physically via van der Waals forces. At elevated temperatures, these molecules dissociate into atoms and dissolve into substrates as an interstitial solid solution [14]. In the next stage, the oxygen atoms produce oxide precipitating and nucleating (homogeneously or in-homogenously) in supersaturated regions of the metal interface, forming a thin oxide film layer; oxygen and metal atoms continuously exchange their positions occupied to produce a very thin suboxide film in a crystalline or amorphous form [15]. From the aspect of a macroscopic viewpoint, oxygen atoms diffusing inwards and titanium atoms diffusing outwards are the two processes controlling continuous oxidation, which produce a $TiO_2$ oxide layer, both at the surface and the interface [16]. The titanium atoms' outward diffusion was further boosted by the assistance of a metal layer, like gold [17]. As oxidation goes, the dense oxide layer and the void impede the outward diffusion of titanium atoms. Therefore, oxygen diffusing inwards dominates the growth of the oxide layer, which is also affected by the dense layer causing a slow oxidation rate [18]. For traditional oxidation, it is relatively fast before the oxide layer forms at the beginning, and then thermal oxidation slows down, as atoms need to diffuse through the oxide layer (Figures 4 and 7) [19,20].

A thin vanadium layer pre-deposited on the surface greatly accelerated CCT due to a large amount of oxygen absorbed, as shown in Table 1. The mass gain of C-V620/8 doubled that of C-620/8, and the thickness of the oxide layer for C-V620/8 was 4~5 times that of C-620/8, as shown in Figure 5a,d. As reported earlier, vanadium tended to promote oxygen diffusion in the oxide layer and led to the formation of oxide at the interface of the oxide and metal [16]. As indicated in Figure 6, the oxidation of CPTi with a pre-deposited vanadium layer at 620 °C was far higher than that of the titanium without the vanadium layer. Extending the treatment time to 80 h, the oxide layer thickness was only 2–3 times the sample without the vanadium layer, as shown in Figure 5b,e and Figure 7. This might be due to the diffusion of oxygen and titanium, which both became slower with the increment of the oxide layer and decreased the oxidation rate at the later stage. It is noticed that although the thickness of the oxide layer increased, the diffusion zone under the oxide layer for the samples with or without the vanadium layer is almost the same after the same CCT, which was still temperature and time dependent, as evidenced in the micro-hardness

profile in Figure 10. The hardened zone under the oxide layer for CCT at 620 °C for 80 h was clearly deeper than that treated for 8 h. This suggested that vanadium only influenced the growth of the oxide layer or the oxygen diffusion in the oxide layer, but did not affect the oxygen diffusion in the substrate. Another impact of vanadium may be attributed to the high solubility of V in the titanium substrate, which facilitated the formation of the $Ti(V)O_2$ solid solution [21]. The $V^{3+}$ ion may replace the position of $Ti^{4+}$ ions to produce V-doped $TiO_2$, increasing the interstitial $Ti^{4+}$ ion content and decreasing the excess electron content to accelerate oxidation. However, only rutile phases were identified on the surface of the oxide layer (Figure 7); although some reports claimed anatase and rutile coexisted when CPTi was subjected to oxidation at temperatures up to 718 °C [22]. There was no clear evidence of the formation of $Ti(V)O_2$, but for sample C-V660/8, the shift of R (110) might be affected by the doping of vanadium. The formation of the rutile $TiO_2$ was expected as the transformation of anatase to the rutile occurs between 400 °C and 500 °C [23], and at temperatures above 600 °C where the rutile $TiO_2$ dominates the oxide formation [24]. Vanadium also seems to favor the rutile phase.

In short, vanadium promotes the adsorption of oxygen and facilitates its diffusion in the oxide layer and, thus, greatly accelerates the oxidation of titanium in CCT.

### *4.2. The Tribological Properties of Vanadium Enriched Oxide Layer*

As reported earlier, titanium alloys are characterized by high chemical activity and plastic flow, which leads to strong adhesion and material transfer resulting in high and unstable friction [25,26]. As shown in Figure 11, the untreated CPTi sample had an extremely unstable and high CoF in the entire test against a WC ball at a load of 40 N. After CCT, all samples had a low initial CoF of 0.1 due to the $TiO_2$ layer formed on the surface [27]. However, the CoF all increased with the increment of test cycles. Without the vanadium layer, the CoF reached a similar level at about 0.3–0.4 through sample C-620/8, which took a short time, while C-660/8 used a longer cycle. The worn track in Figures 13a and 14a,c suggests that the oxide layer was cut through at a certain stage and some oxide debris played an important role in the tribo-test, which led to a higher friction value. Although the oxide layer formed on the surface became much harder (Figure 9), which may benefit from reducing wear, the hard debris created in the test from the delaminated or broken oxides (Figure 12a) could hinder the movement of the counterpart ball, which increased the friction.

For the vanadium pre-deposited sample, only the C-V620/8 sample maintained a relatively lower and stable CoF under 0.3 after the surge began (Figure 11), the other two samples of C-V620/80 and C-V660/8 had a firm increase of friction till the end of the test, which was even higher than that of the untreated samples. The hydrophobic titanium surface with a macro-nano structure was reported to reduce friction as wetting properties would change the adhesion of the friction surface [28]. A larger contact angle could decrease the adhesion and reduce the CoF; however, it might increase the wear mass. The higher contact angle of C-V620/8 among the V pre-deposited samples (Figure 15) may partly account for its lower and stable friction, as seen in Figure 11. Furthermore, the high contact angle of the titanium surface without V after CCT may be responsible for their relatively lower friction. Good wettability may benefit from improved lubrication [29] and enhance the tribological performance [30,31], which needs to be further explored. The oxide layer in the track was all cut through and delaminated partially, as seen in Figures 13b and 14b,d. The wear area was also remarkably higher than those without a vanadium layer, this might be due to the slightly harder surface (Figure 9), which produced some harder particles and enhanced the friction and wear. Another reason could be due to the surface oxide layer not being very dense, as seen in Figure 5e,f.

In short, it is necessary to generate a thin oxide layer (less than 4 μm) on the surface, such as C-V620/8, to obtain low and stable friction, and the oxide layer needs to be dense and compact to acquire high wear resistance. Therefore, it will be interesting to test samples CCTed at shorter times to further improve the tribological properties of the titanium alloys.

## 5. Conclusions

The effect of the pre-deposited vanadium layer on the oxidation of CPTi under three CCT conditions (620 °C for 8 h, 660 °C for 8 h, and 620 °C for 80 h) was investigated. The following conclusions can be drawn:

1. A thin pre-deposited V layer brought about a significantly accelerated CCT of CPTi regarding the thickness of the oxide layer.
2. Generally, rutile titanium dioxide was formed on the surface and vanadium assisted the growth of the rutile phase.
3. CCT drastically increased the surface hardness, which was further reinforced after a long duration of 80 h. Longer treatment or higher temperatures created a deep hardened zone or oxygen diffusion zone.
4. All CCTed samples had low wear, but the friction depended on the oxide layer quality and thickness. A dense and compact oxide layer with a suitable thickness was needed for better overall tribological properties.
5. The oxide layer formed on the surface of titanium generally increased the contact angle, but vanadium in the oxide layer reduced the contact angles significantly and, therefore, improved the wettability.

**Author Contributions:** Conceptualization, Z.Z.; methodology, Z.Z.; validation, R.D. and Z.Z.; formal analysis, R.D. and Z.Z.; investigation, R.D.; resources, Z.Z. and H.D.; data curation, Z.Z. and R.D.; writing—original draft preparation, Z.Z.; writing—review and editing, Z.Z.; supervision, H.D.; project administration, Z.Z.; funding acquisition, H.D. All authors have read and agreed to the published version of the manuscript.

**Funding:** This research received no external funding.

**Data Availability Statement:** Data available on request.

**Conflicts of Interest:** The authors declare no conflict of interest.

## References

1. Yang, J.; Liu, C.; Sun, H.; Liu, Y.; Liu, Z.; Zhang, D.; Zhao, G.; Wang, Q.; Yang, D. The progress in titanium alloys used as biomedical implants: From the view of reactive oxygen species. *Front. Bioeng. Biotechnol.* **2022**, *10*, 1092916. [CrossRef]
2. Pushp, P.; Dasharath, S.M.; Arati, C. Classification and applications of titanium and its alloys. *Mater. Today Proc.* **2022**, *54*, 537–542. [CrossRef]
3. Philip, J.T.; Mathew, J.; Kuriachen, B. Tribology of Ti6Al4V: A review. *Friction* **2019**, *7*, 497–536. [CrossRef]
4. Zhang, L.-C.; Chen, L.-Y.; Wang, L. Surface Modification of Titanium and Titanium Alloys: Technologies, Developments, and Future Interests. *Adv. Eng. Mater.* **2020**, *22*, 1901258. [CrossRef]
5. Chouirfa, H.; Bouloussa, H.; Migonney, V.; Falentin-Daudré, C. Review of titanium surface modification techniques and coatings for antibacterial applications. *Acta Biomater.* **2019**, *83*, 37–54. [CrossRef] [PubMed]
6. Zhang, Z.X.; Dong, H.; Bell, T.; Xu, B.S. The effect of deep-case oxygen hardening on the tribological behaviour of a-C:H DLC coatings on Ti6Al4V alloy. *J. Alloys Compd.* **2008**, *464*, 519–525. [CrossRef]
7. Guleryuz, H.; Cimenoglu, H. Surface modification of a Ti–6Al–4V alloy by thermal oxidation. *Surf. Coat. Technol.* **2005**, *192*, 164–170. [CrossRef]
8. Zhang, Z.; Zhang, Y.; Tao, X.; Liu, K.; Burns, A.; Li, P.; Mukinay, T.; Li, X.; Dong, H. The exceptional oxidation of Ti6Al4V alloy with a pre-deposited silver layer. *J. Alloys Compd.* **2022**, *901*, 163574. [CrossRef]
9. Zhang, Z.; Zhang, Y.; Li, X.; Alexander, J.; Dong, H. An enhanced ceramic conversion treatment of Ti6Al4V alloy surface by a pre-deposited thin gold layer. *J. Alloys Compd.* **2020**, *844*, 155867. [CrossRef]
10. Senopati, G.; Rahman Rashid, R.A.; Kartika, I.; Palanisamy, S. Recent Development of Low-Cost β-Ti Alloys for Biomedical Applications: A Review. *Metals* **2023**, *13*, 194. [CrossRef]
11. Uwanyuze, R.S.; Alpay, S.P.; Schafföner, S.; Sahoo, S. A first principles analysis of oxidation in titanium alloys with aluminum and vanadium. *Surf. Sci.* **2022**, *719*, 122026. [CrossRef]
12. Takahashi, T.; Minamino, Y.; Hirasawa, H.; Ouchi, T. High-Temperature Oxidation and Its Kinetics Study of Ti–Al and Ti–V Alloys in Air. *Mater. Trans.* **2014**, *55*, 290–297. [CrossRef]
13. Lu, J.; Huang, T.; Liu, Z.; Zhang, X.; Xiao, R. Long-term wettability of titanium surfaces by combined femtosecond laser micro/nano structuring and chemical treatments. *Appl. Surf. Sci.* **2018**, *459*, 257–262. [CrossRef]
14. Kofstad, P. High-temperature oxidation of titanium. *J. Less Common Met.* **1967**, *12*, 449–464. [CrossRef]
15. Du, H.L.; Datta, P.K.; Lewis, D.B.; Burnell-Gray, J.S. Air oxidation behaviour of Ti6Al4V alloy between 650 and 850°. *Corros. Sci.* **1994**, *36*, 631–642. [CrossRef]

16. Salomonsen, G.; Norman, N.; Lønsjø, O.; Finstad, T.G. Kinetics and mechanism of oxide formation on titanium, vanadium and chromium thin films. *J. Less Common Met.* **1990**, *158*, 251–265. [CrossRef]
17. Zhang, Z.; Yu, H.; Li, X.; Dong, H. Impact of the Amount of the Gold Layer on the Tribological Performance of the Ceramic Conversion Treated CP-Titanium. *Tribol. Lett.* **2023**, *71*, 36. [CrossRef]
18. Bakulin, A.V.; Chumakova, L.S.; Kulkova, S.E. Study of the Diffusion Properties of Oxygen in $TiO_2$. *J. Exp. Theor. Phys.* **2021**, *133*, 169–174. [CrossRef]
19. Vaché, N.; Cadoret, Y.; Dod, B.; Monceau, D. Modeling the oxidation kinetics of titanium alloys: Review, method and application to Ti-64 and Ti-6242s alloys. *Corros. Sci.* **2021**, *178*, 109041. [CrossRef]
20. Estupinán-López, F.; Orquiz-Muela, C.; Gaona-Tiburcio, C.; Cabral-Miramontes, J.; Bautista-Margulis, R.G.; Nieves-Mendoza, D.; Maldonado-Bandala, E.; Almeraya-Calderón, F.; Lopes, A.J. Oxidation Kinetics of Ti-6Al-4V Alloys by Conventional and Electron Beam Additive Manufacturing. *Materials* **2023**, *16*, 1187. [CrossRef]
21. Fernandes, F.; Morgiel, J.; Polcar, T.; Cavaleiro, A. Oxidation and diffusion processes during annealing of TiSi(V)N films. *Surf. Coat. Technol.* **2015**, *275*, 120–126. [CrossRef]
22. Gemelli, E.; Camargo, N.H.A. Oxidation kinetics of commercially pure titanium. *Matéria* **2007**, *12*, 525–531. [CrossRef]
23. Depero, L.E.; Bonzi, P.; Zocchi, M.; Casale, C.; De Michele, G. Study of the anatase-rutile transformation in $TiO_2$ powders obtained by laser-induced synthesis. *J. Mater. Res.* **1993**, *8*, 2709–2715. [CrossRef]
24. Mungole, M.N.; Singh, N.; Mathur, G.N. Oxidation behaviour of Ti6Al4V titanium alloy in oxygen. *Mater. Sci. Technol.* **2002**, *18*, 111–114. [CrossRef]
25. Su, J.; Xie, H.; Tan, C.; Xu, Z.; Liu, J.; Jiang, F.; Tang, J.; Fu, D.; Zhang, H.; Teng, J. Microstructural characteristics and tribological behavior of an additively manufactured Ti-6Al-4V alloy under direct aging and solution-aging treatments. *Tribol. Int.* **2022**, *175*, 107763. [CrossRef]
26. Khan, I. Improving the Cytocompatibility and Infection, Wear and Corrosion Resistances of Commercially Pure Titanium by Laser Micropatterning and Ceramic Conversion Treatment. Ph.D. Thesis, The University of Birmingham, Birmingham, UK, 2020.
27. Ilie, F.; Ipate, G.; Manaila, F.C. Tribological Properties Study of Solid Lubrication with $TiO_2$ Powder Particles. *Materials* **2022**, *15*, 7145. [CrossRef]
28. Huang, J.; Cai, L.; Zhang, W.; Zhang, L.; Jiang, B.; Kong, L. Influence of surface structure/wettability on tribological properties of titanium. *Tribol. Int.* **2022**, *174*, 107747. [CrossRef]
29. Borruto, A.; Crivellone, G.; Marani, F. Influence of surface wettability on friction and wear tests. *Wear* **1998**, *222*, 57–65. [CrossRef]
30. Acar, M.T.; Kovacı, H.; Çelik, A. Enhancement of the tribological performance and surface wettability of Ti6Al4V biomedical alloy with boric/sulfuric acid anodic film. *Surf. Topogr. Metrol. Prop.* **2021**, *9*, 035024. [CrossRef]
31. Jia, D.; Zhang, Y.; Li, C.; Yang, M.; Gao, T.; Said, Z.; Sharma, S. Lubrication-enhanced mechanisms of titanium alloy grinding using lecithin biolubricant. *Tribol. Int.* **2022**, *169*, 107461. [CrossRef]